

University of Groningen

## Scaling of the failure stress of homophase and heterophase three-dimensional spring networks

Chung, J.W; de Hosson, J.T.M.; van der Giessen, E.

*Published in:*  
Physical Review B

*DOI:*  
[10.1103/PhysRevB.65.094104](https://doi.org/10.1103/PhysRevB.65.094104)

**IMPORTANT NOTE:** You are advised to consult the publisher's version (publisher's PDF) if you wish to cite from it. Please check the document version below.

*Document Version*  
Publisher's PDF, also known as Version of record

*Publication date:*  
2002

[Link to publication in University of Groningen/UMCG research database](#)

### *Citation for published version (APA):*

Chung, J. W., de Hosson, J. T. M., & van der Giessen, E. (2002). Scaling of the failure stress of homophase and heterophase three-dimensional spring networks. *Physical Review B*, 65(9), art - 094104. [094104]. <https://doi.org/10.1103/PhysRevB.65.094104>

### **Copyright**

Other than for strictly personal use, it is not permitted to download or to forward/distribute the text or part of it without the consent of the author(s) and/or copyright holder(s), unless the work is under an open content license (like Creative Commons).

The publication may also be distributed here under the terms of Article 25fa of the Dutch Copyright Act, indicated by the "Taverne" license. More information can be found on the University of Groningen website: <https://www.rug.nl/library/open-access/self-archiving-pure/taverne-amendment>.

### **Take-down policy**

If you believe that this document breaches copyright please contact us providing details, and we will remove access to the work immediately and investigate your claim.

Downloaded from the University of Groningen/UMCG research database (Pure): <http://www.rug.nl/research/portal>. For technical reasons the number of authors shown on this cover page is limited to 10 maximum.

# Scaling of the failure stress of homophase and heterophase three-dimensional spring networks

J. W. Chung, J. Th. M. De Hosson,\* and E. van der Giessen

*Department of Applied Physics, Materials Science Centre and Netherlands Institute of Metals Research, University of Groningen, Nijenborgh 4, 9747 AG Groningen, The Netherlands*

(Received 18 July 2001; published 1 February 2002)

This paper concentrates on the scaling of the failure stress of a three-dimensional spring network as a function of its volume. In particular, the influences of the geometry and the local structure are examined. Both homophase disordered three-dimensional structures and composite systems are studied, containing a more or less ordered slab. The structures are generated by starting with a node distribution. A molecular-dynamics-based algorithm uses void volume spheres, which all have Lennard-Jones interacting outer surfaces. The generated distributions of nodes form the basis of a procedure to interconnect the nodes with springs. In the calculation of the failure stress the total elastic energy is described by two-body central force, three-body bond bending, and four-body torsion contributions. The areas under uniaxial compression are varied in the range of  $0.64\text{--}5.76\ \mu\text{m}^2$ , and the height  $h$  ranges between  $0.80$  and  $6.4\ \mu\text{m}$ . It is found that the failure stress at constant base area could be described by  $\sigma_{\text{fail}} \propto [\log(h/\xi)]^{-1/\mu}$ , where  $\xi$  represents the correlation length within the sample (the logarithm is to the base  $e$ ). The values of  $\mu$  are effective values. Only within the same kind of failure mechanism and microstructure does the exponent  $\mu$  become more or less universal. Actually, the modulus  $\mu$  appears to depend on the system size, but in all cases thin samples are stronger than thick samples under uniaxial compression, and the failure stress increases with increasing coordination number. The failure stress of heterophase materials differs considerably in our calculations from that of homophase materials. The composite materials exhibit an increase in strength by a factor of 4, in comparison to the disordered structures of the same size. The actual failure stress of the composite material depends critically on the layering effect of the disordered region near the ordered phase.

DOI: 10.1103/PhysRevB.65.094104

PACS number(s): 46.50.+a

## I. INTRODUCTION

The basic question addressed in this paper is the following: what is the difference in strength between a large disordered structure and a small structure loaded under uniaxial compression? If the material is perfectly homogeneous, no particular difference in local stress and strain fields will be observed. An infinite linear elastic material would even be infinitely strong, and such a system could support arbitrarily large loads. To predict, within a physical description, a limit in strength, a certain nonlinearity has to be considered, such as cracks that extend under an increasing mechanical load. These defects make the material essentially nonlinear, even for perfectly linear elastic systems. For finite systems, size effects on the failure stress come about as a direct consequence of the existence of defects such as cracks on a microscale. If a difference in strength is encountered as a function of size it is due to the fact that the proportion between the length scale at which fracture originates and propagates with respect to the macroscopic size of the structure alters if the size is enlarged. Therefore, the ability to accommodate local failure, i.e., a redistribution of mechanical energy in the local surroundings, does not depend only on the intrinsic material properties, but also on extrinsic factors such as boundary conditions and the size and geometry of the specimen.

This paper concentrates on the fracture behavior of highly porous disordered media, so as to mimic ceramic extrudates that are commonly used as catalyst carriers. The porosity of these extrudates is about 70 vol %. In particular, catalyst carriers should also be strong enough to withstand the applied

load under operating conditions of a (petro)chemical plant.<sup>1</sup> The main objective in this field of research is to access by a modeling approach how microstructural features affect the final failure distribution. Elastic networks of springs are frequently used to model the relation between the mechanical properties and the microstructure of (highly) porous media. In this work disordered three-dimensional spring networks<sup>2,3</sup> are used to study the size effect in brittle failure. In the past simulations were carried out both in two<sup>4–7</sup> and three<sup>8–13</sup> dimensions, mainly exploring regular spring networks. In general, so far the research on size effects<sup>14,15</sup> and fracture growth<sup>16</sup> seemed to underline the importance of heterogeneities in random resistor network models.<sup>17</sup> Further, experimental and numerical investigations of size effects were pursued in the field of concrete fracture mechanics using deterministic models.<sup>18,19</sup>

In order to incorporate a specific microstructure of highly porous ceramic media, we explore a method of dynamically generating a node distribution. This rather mesoscopic approach provides the possibility to incorporate microstructural properties. It is important to realize that any strength distribution during the fracturing process is due to the node distribution itself. Thus even a homophase sample may not be homogeneous in strength on either a local or global scale.

## II. COMPUTATIONAL PROCEDURE

### A. Generation of network

The computational procedure starts with the generation of a node distribution. The molecular-dynamic-based algorithm uses  $N$  void volume spheres, which all have Lennard-Jones

interacting outer surfaces. The method provides a convenient way of generating a distribution of disordered nodes. The disorder is controlled by the preset values of the temperature and pressure thermostat.<sup>20</sup> The radii of the void volume spheres are taken 25 nm, and the Lennard-Jones<sup>21</sup> outer surface interaction,  $\sigma_{LJ}$ , is also set to 25 nm. The temperature of the reference bath is  $8.0\varepsilon/k_B$  ( $0.78\varepsilon/k_B$  is the Lennard-Jones triple point temperature with  $\varepsilon$  the energy, and  $k_B$  is Boltzmann's constant), and the pressure reference bath is pre-set to the value of  $0.4\varepsilon/\sigma_{LJ}^3$  (1.275 is the Lennard-Jones triple point pressure). Those values are found to be sufficient to generate a disordered spatial distribution<sup>22</sup> of particles.

The relaxation process took 25 000 time steps in order to attain equilibrium using a time increment step  $\Delta t$  of  $10^{-9}$  s. The leap-frog integration scheme<sup>18</sup> calculates the position and velocities of the particles using Newtonian equations of motion. The driving force for each particle in each step is a superposition of all the interactions of the particle with its neighboring particles. After the first 20 000 time steps, eight node distributions are sampled. All the distributions are taken with 2000 consecutive time steps in between. For each combination of width:depth:height, in total nine distribution are generated to attain a better representation of the equilibrated disordered system.

The thermostat maintains a constant pressure in the mesoscopic particle system, achieving this by adjusting the box size. To remove the effect of the node density all the node distributions are scaled to an average node density of 500 nodes/ $\mu\text{m}^3$ , resulting in an average spacing in three dimensional of 0.125  $\mu\text{m}$ .

The generated distributions form the basis of the spring connecting procedure. Every node is a potential point of connection, and as a consequence the geometry of the network is globally fixed by the positions of the nodes. Actually, only the interaction length between the nodes is left as a parameter. The node interaction between two nodes exists only if their relative distance is below the connectivity threshold  $C_t$ . Depending on the value of  $C_t$ , the system may develop from fully connected, i.e., every node is connected with all the other nodes, to a lower limit where all nodes are disconnected. For low  $C_t$  the network resembles a Delaunay network, whereas for higher  $C_t$  values the network geometry will deviate more and more from it. In this investigation  $C_t$  is 0.15  $\mu\text{m}$ . This value is one of the lowest  $C_t$  value that could be addressed, while remaining a network with a constant average node density.

### B. Compression of network

In the following the spring networks are loaded in compression and after each force increment, the network configuration with the lowest energy is calculated. The total elastic energy is described by a two-body central force (CF), a three-body bond bending (BB), and a four-body torsion (T) contribution<sup>3</sup>

$$U_{EL} = U_{CF} + U_{BB} + U_T. \quad (2.1)$$

The central force contribution on node  $i$ ,  $\Delta F_i^{CF}(n+1)$  with respect to the previous force,  $\Delta F_i^{CF}(n)$ , is given by the

first derivative of the central force potential  $U_{CF}$  with respect to the node position of  $i$ ,  $q_i$ , i.e.,

$$\begin{aligned} \Delta F_i^{CF}(n+1) &= -1 \left[ -\frac{\partial U_{CF}(n+1)}{\partial q_i} \right] \\ &= -k_{ij}^{CF} [\Delta \mathbf{u}_{ij}(n+1) \cdot \hat{\mathbf{R}}_{ij}(n)] \hat{\mathbf{R}}_{ij}^q(n), \end{aligned} \quad (2.2)$$

where the CF potential is described by

$$\begin{aligned} U_{CF}(n+1) &= \frac{1}{2} \sum_{\langle ij \rangle} k_{ij}^{CF} [\Delta \mathbf{u}_{ij}(n+1) \cdot \hat{\mathbf{R}}_{ij}(n) \\ &\quad + (|\mathbf{R}_{ij}(n)| - |\mathbf{R}_{ij}(0)|)^2], \end{aligned} \quad (2.3)$$

$\langle ij \rangle$  denotes the summation over all  $ij$  pairs of connected nodes. The bond vector  $\mathbf{R}_{ij}(n)$  from node  $i$  to node  $j$  ( $\equiv$  bond  $ij$ ) at an increment  $n$  is defined as  $\mathbf{R}_{ij}(n) = \mathbf{r}_j(n) - \mathbf{r}_i(n)$ , ( $\hat{\mathbf{R}}_{ij} = \mathbf{R}_{ij}/|\mathbf{R}_{ij}|$ ), where  $\mathbf{r}_j(n)$  is the position of node  $j$  at increment  $n$ . Furthermore, the displacement increment  $\Delta \mathbf{u}_{ij}(n)$  at increment  $n$  is given by  $\Delta \mathbf{u}_{ij}(n) = \Delta \mathbf{u}_j(n) - \Delta \mathbf{u}_i(n)$ , where  $\Delta \mathbf{u}_i(n) \equiv \mathbf{u}_i(n+1) - \mathbf{u}_i(n)$  is the bond displacement increment of node  $i$  and  $\mathbf{u}_i(n) \equiv \mathbf{r}_i(n) - \mathbf{r}_i(0)$  represents the displacement of node  $i$  at increment  $n$ . The force constant for the CF follows from the uniaxial straining of a bar of length  $|\mathbf{R}_{ij}(0)|$ , with Young's modulus  $E$  and cross-sectional area  $A_{ij}$ :

$$k_{ij}^{CF} = \frac{A_{ij}E}{|\mathbf{R}_{ij}(0)|}, \quad (2.4)$$

The magnitude of the force constant is inversely proportional to the initial bond length.

For the bond bending potential (the three-body term) between nodes  $ijk$ , where  $i$  is the center of the hingelike bond bending potential  $U_{BB}$ , the following expression is used:

$$\begin{aligned} U_{BB}(n+1) &= \frac{1}{2} \sum_{\langle ijk \rangle} k_{ijk}^{BB} [\Delta \theta_{ijk}^{ij}(n+1) + \Delta \theta_{ijk}^{ik}(n+1) \\ &\quad + \theta_{ijk}(n)]^2. \end{aligned} \quad (2.5)$$

$\Delta \theta_{ijk}^{ij}(n+1)$  and  $\Delta \theta_{ijk}^{ik}(n+1)$  are the angular deviations in step  $n+1$ , due to the beamlike bending of bonds  $ij$  and  $ik$ . The force constant

$$k_{ijk}^{BB} = \left( \frac{1}{k_{ijk}^{ij}} + \frac{1}{k_{ijk}^{ik}} \right)^{-1}, \quad (2.6)$$

with  $k_{ijk}^{ij}$  and  $k_{ijk}^{ik}$  taken from the elasticity theory of a bending beam. The first component is given by

$$k_{ijk}^{ij} = \frac{3EI_{ij}}{|\mathbf{R}_{ij}(n)|}, \quad (2.7)$$

with  $I_{ij}$  is the second moment of area of bond  $ij$ . The second one  $k_{ijk}^{ik}$  of bond  $jk$  is found similarly.

The torsion interaction  $U_T$  along the bond  $ik$ , due to the relative motions of bond  $ij$  and bond  $kl$ , is a pseudo-four-body potential. When bonds  $ij$  and  $kl$  are projected onto a

plane normal in the direction of bond  $ik$ , this yields a three-body problem  $j-i-k-l \rightarrow (j-i'-l)$ , with  $i'=(ik)$ . The torsion potential is therefore actually a  $(ik)jl$  bond bending potential in the  $ik$  plane, where  $(ik)$  stands for the point in the  $ik$  plane where bond  $ik$  intersects the  $ik$  plane. The potential can now be written as

$$U_T(n+1) = \frac{1}{2} \sum_{\langle ijkl \rangle} k_{ijkl}^T [\Delta \phi'_{ijkl}(n+1) + \phi_{ijkl}(n)]^2 \quad (2.8)$$

and  $\phi_{ijkl}$  is the angle in the  $ik$ -plane-projected system. As for bond bending, the torsion force constant is taken from elasticity theory, and is defined as

$$k_{ijkl}^T = \frac{EI_{ik}}{(1+\nu)|\mathbf{R}_{ik}(n)|}, \quad (2.9)$$

where  $\nu$  is Poisson's ratio.

When all the node-node interactions are added into the global matrix, a system of  $3N$  ( $N$  being the number of spheres) linear equations is formed, or  $\Delta \mathbf{F}(n+1) = [K]\Delta \mathbf{u}(n+1)$ , where  $\Delta \mathbf{F}(n+1)$  is a  $3N$ -dimensional vector of the applied force increments at compression step  $n$ ,  $[K]$  the  $3N \times 3N$  stiffness matrix, and  $\Delta \mathbf{u}(n+1)$   $3N$ -dimensional vector of the displacement increments in the compression step  $n$ . Indeed, normally when torsional forces are included in the force balance the number of the equations to be solved for a 3D system of  $N$  nodes (or spheres) is  $6N$  (three for the displacements and three for the rotations). The  $3N$  case would be possible only if the torsional interactions are related, as stated above, to the displacements of actually a three-body bond-bending potential. By projecting bonds  $ij$  and  $kl$  onto the plane normal in the direction of bond  $ik$  (also see Fig. 4 in Ref. 3) the torsion angle increment  $\Delta \phi_{ijkl}(n+1) = \phi_{ijkl}(n+1) - \phi_{ijkl}(n)$  in Eq. (2.8), with  $\phi_{ijkl}(n)$  the total change of torsion angle of bond  $ik$  at increment  $n$  relative to the initial torsion angle [i.e.,  $\phi_{ijkl}(0) \equiv 0$ ] can be written as

$$\begin{aligned} \Delta \phi_{ijkl}(n+1) &= \Delta \mathbf{u}_{ij}(n+1) \\ &\cdot \left( \frac{\hat{\mathbf{R}}_{ij}(n) \times \hat{\mathbf{R}}_{ik}(n)}{|\mathbf{R}_{ij}(n)| |\{1 - [\hat{\mathbf{R}}_{ij}(n) \cdot \hat{\mathbf{R}}_{ik}(n)]^2\}|} \right) \\ &+ \Delta \mathbf{u}_{kl}(n+1) \\ &\times \left( \frac{\hat{\mathbf{R}}_{ik}(n) \times \hat{\mathbf{R}}_{kl}(n)}{|\mathbf{R}_{kl}(n)| |\{1 - [\hat{\mathbf{R}}_{kl}(n) \cdot \hat{\mathbf{R}}_{ik}(n)]^2\}|} \right). \end{aligned} \quad (2.10)$$

The angle change  $\phi_{ijkl}(n)$  is given by

$$\phi_{ijkl}(n) = \arccos[\hat{\mathbf{r}}_{kl}(n) \cdot \hat{\mathbf{r}}_{ij}(n)] - \arccos[\hat{\mathbf{r}}_{kl}(0) \cdot \hat{\mathbf{r}}_{ij}(0)]. \quad (2.11)$$

The external force is applied through the force vector. The resulting displacement increments are obtained by solving the system of equations using a preconditioned conjugate gradient algorithm which exploits the fact that  $[K]$  is a

TABLE I. Overview of the total number of configurations examined for a particular combination of base area and height.

Height ( $\mu\text{m}$ ) Base ( $\mu\text{m}^2$ )	0.8	1.2	1.6	2.4	3.2	4.8	6.4
0.64	9	9	8	8	9		
1.44	8	9	8	8	8	10	5
2.56	8	8	7	7	6	8	4
5.76	6	3	8	3	5	3	

sparse matrix. The positions at the end of increment  $n+1$  are updated according to  $\mathbf{r}_i(n+1) = \mathbf{r}_i(n) + \Delta \mathbf{u}_i(n+1)$ .

The fracture criterion used throughout this work is the maximum strain of 0.25%. The same value is also applied as a fracture criterion for the bond length and angular distortion. Once the fracture strain is satisfied in a spring element, the bond is removed from the network. Nodes without connection (floating nodes) or groups of unconnected nodes (fragments) are also removed from the interaction matrix. As a result of the removal of floating nodes and fragments, the possible effects of these fragments on the actual failure stress are explicitly ignored. An exception is maintained for the first layer on the top at the sample and the last layer on the bottom of the sample with a thickness of 10 nm. All connections emerging from nodes lying within these two layers are not subjected to fracture. This is done to take into account the fragmentation effect at the contact area. Actually, these unremoved nodes will effectively transmit the load similar to the ability of the fragments to transmit the load in real experiments.

### III. RESULTS

Various specimens with different base areas are constructed, namely, 0.64, 1.44, 2.56, and  $5.76 \mu\text{m}^2$ . In addition, the size effect is explored by generating samples of different heights, thus leading to different aspect ratios. The various configurations are listed in Table I. An example of an intermediate stage in the fracturing process is displayed in Fig. 1 (a base area  $2.56 \mu\text{m}^2$  and a height of  $2.4 \mu\text{m}$ ). The radius of the cross section of the bonds in the network is  $0.1 \mu\text{m}$  and the Young's modulus is set to be 400 GPa. Throughout the calculations the node density is kept constant, that is 500 nodes per  $\mu\text{m}^3$ . Using these properties the calculations lead to a failure stress of the order of 10 MPa, which is reasonable for highly porous ceramic materials.<sup>23</sup>

The overall volume effect on the failure stress,  $\sigma_{\text{fail}}$ , shows a Weibull<sup>24</sup> behavior, as depicted in Fig. 2. Here and in the following the logarithm is to base  $e$ . In the weakest-link assumption of Weibull, fracture initiation leads to immediate global failure. The probability  $g(\sigma)$ , that fracture will initiate locally at a stress  $\sigma$ , is described by a power-law behavior  $g(\sigma) = \sigma^m$ , where  $m$  is the so-called Weibull modulus reflecting the materials properties. The cumulative failure distribution is expressed by

$$F_V(\sigma) = 1 - e^{-cL^d\sigma^m} \quad (3.1)$$



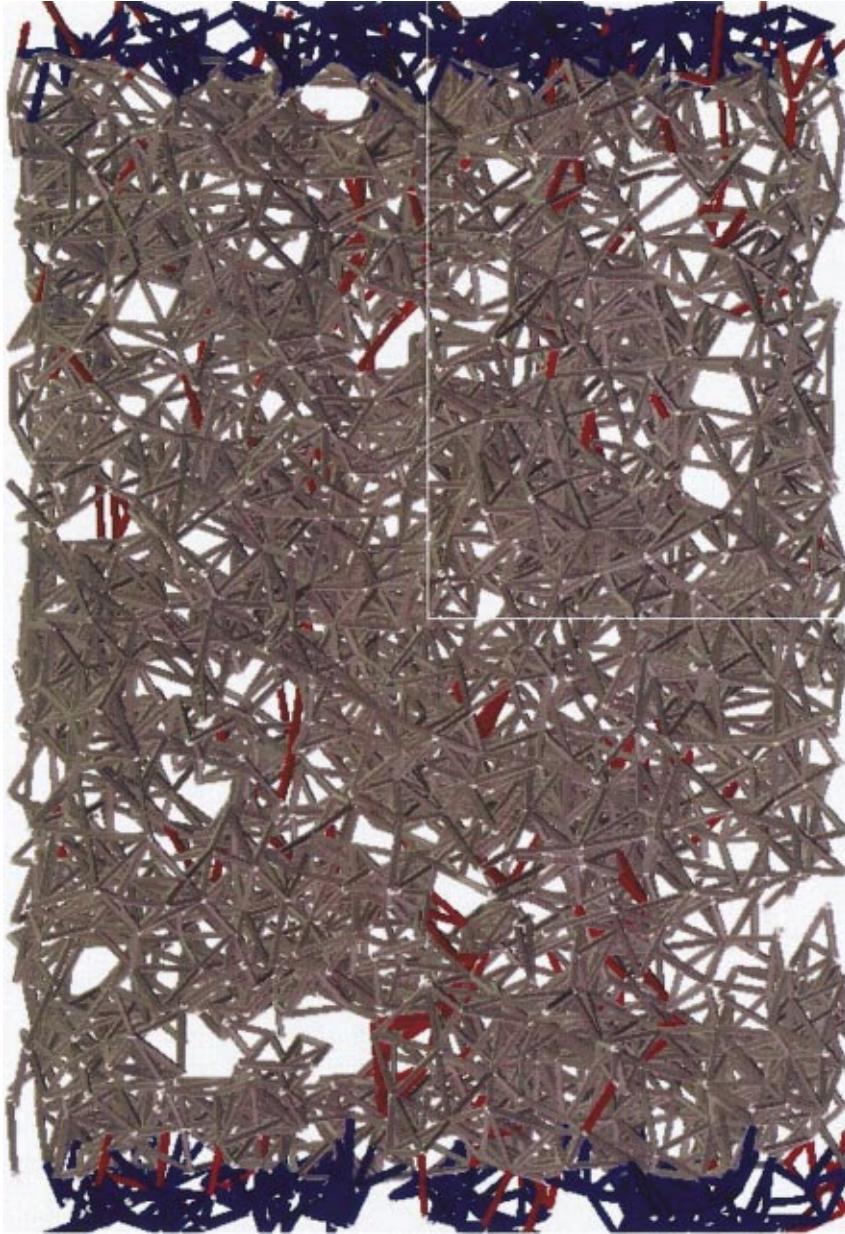


FIG. 1. (Color) Intermediate stage in the fracturing process of a sample with a base area of  $2.56 \mu\text{m}^2$  and a height of  $2.4 \mu\text{m}$ . Red bonds fulfill the fracture criterion.

for a volume  $L^d$ , where  $c$  is a geometrical constant and  $d$  represents the dimensionality. The cumulative failure probability goes to unity for  $\sigma \rightarrow \infty$ . However, if the sample size increases,  $F(\sigma)$  shifts toward lower values of  $\sigma$  and the failure probability becomes of the order of unity for even smaller values of the stress. The expectation value of the failure distribution  $\sigma_{\text{fail-W}}$  (taken here as the median value) predicts a dependence of the failure stress on the size according to  $\sigma_{\text{fail-W}} \sim L^{-d/m}$  for a  $d$ -dimensional space of linear size  $L$ .

Figure 3 displays the volume dependence of failure stress according to the description based on extreme statistics as developed by Leath and Duxbury<sup>16</sup> and Chakrabarti and co-workers.<sup>25,26</sup> Although it also based on a weakest-link assumption, here the chance that fracture will initiate locally at a stress  $\sigma$  is described by

$$g(\sigma) = e^{-k/\sigma^\mu}, \quad (3.2)$$

leading to a failure distribution of the form

$$F_V = 1 - \exp\left[-cL^d \exp\left(-\frac{k}{\sigma^\mu}\right)\right], \quad (3.3)$$

and an expectation value  $\sigma_{\text{fail-D-L}} = k^{1/\mu}(\log L^d + \log c - \log \log 2)^{-1/\mu}$ . It is interesting to note that the failure of hierarchical structures of fiber bundles under equal load sharing<sup>27</sup> leads to  $\sigma_{\text{fail}} \sim (\log \log L^d)^{-1}$ . As in the Weibull case, for extremely large size  $L$ ,  $F(\sigma) \cong 1$  for nonvanishing stress. It may be noted that although in the Weibull distribution the failure probability is unity as  $\sigma \rightarrow \infty$  for any size, this is not necessarily the case for Eq. (3.3), unless the system size becomes very large. The analyses of Ref. 16 and Refs. 25 and 26 are related to the Gumbel<sup>28</sup> form used in fracture reliability analysis. However, the latter is based on a weakest-link argument that assumes that all parts of the material carry the same stress. Equations (3.2) and (3.3) assume

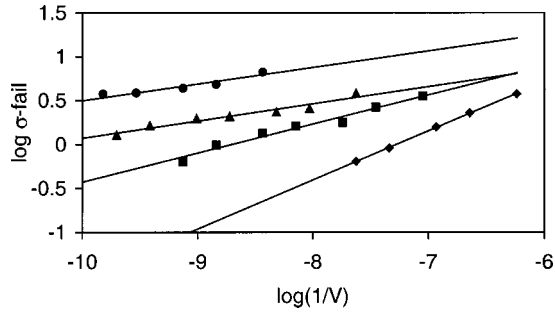


FIG. 2. Double (natural) log plot of failure stress (MPa) vs reciprocal volume (in units of  $10^{-3} \mu\text{m}^3$ ) for various base areas ( $\diamond$ ,  $0.64 \mu\text{m}^2$ ;  $\blacksquare$ ,  $1.44 \mu\text{m}^2$ ;  $\blacktriangle$ ,  $2.56 \mu\text{m}^2$ ;  $\bullet$ ,  $5.76 \mu\text{m}^2$ ).

that failure is initiated by load hotspots. Actually, in contrast to earlier studies,<sup>4,23</sup> the results displayed in Figs. 2 and 3 do not validate either the Gumbel distributions or the Weibull distributions.

The effect of the volume on the failure stress is strongly affected by the local coordination number  $C_{\text{Dis}}$  of the disordered phase. The latter increases with increasing base area (see Table II). As expected, the failure stress also increases with increasing coordination number. In addition to a homophase material represented by a distribution of disordered nodes, composite materials are also studied. They are composed of a slab with thickness  $d_s$  of an ordered material that separates two regions of a disordered phase. The base area is kept constant, being  $0.64 \mu\text{m}^2$ . Figure 4 displays the density as a function of the height and indicates the position of the slice of the ordered material. In Table III, the coordination number of the slab,  $C_s$ , is estimated by assuming the following relationship:  $hC = d_s C_s + (h - d_s) C_{\text{Dis}}$ . The failure stress of the composite materials differs considerably from that of the homophase materials (see Table IV). In fact, the composite materials show an increase in strength by a factor of 4, in comparison to the disordered structures of the same size, i.e., even if the composite phase is compared with the homophase specimens of the effective height,  $h_{\text{eff}} = h - h_{\text{slab}}$ .

#### IV. DISCUSSION AND CONCLUSIONS

Generally speaking, the size effect on the failure stress of disordered networks studied here can be described equally

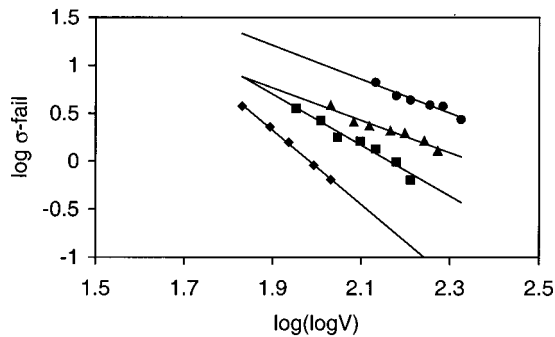


FIG. 3. Double (natural) log plot of failure stress (MPa) vs the natural logarithm of the sample volume (in units of  $10^{-3} \mu\text{m}^3$ ) for various base areas ( $\diamond$ ,  $0.64 \mu\text{m}^2$ ;  $\blacksquare$ ,  $1.44 \mu\text{m}^2$ ;  $\blacktriangle$ ,  $2.56 \mu\text{m}^2$ ;  $\bullet$ ,  $5.76 \mu\text{m}^2$ ).

TABLE II. Coordination number and the parameters  $\mu$  for homophase materials.

Base area ( $\mu\text{m}^2$ )	0.64	1.44	2.56	5.76
Coordination number	3.03	3.16	3.22	3.8
$C_{\text{Dis}}$				
Standard deviation $C_{\text{Dis}}$	0.07	0.07	0.08	0.07
$\mu$	0.66	1.01	1.69	1.82

well by both the Weibull and Gumbel failure distributions. Although the failure stress depends on the volume, the precise geometry of the specimen proves to be an important factor as well. The size effect is stronger for lower coordination numbers, and it seems to diminish for larger values of the coordination number. A quantitative influence of the height on the failure stress can be estimated as follows. The probability  $P$  of a defect of a certain size  $n$  in a volume  $L^d$  can roughly be estimated by  $P(n) \cong L^d p^n$  (with a site probability  $p$ ).<sup>29</sup> Because the probability of a largest defect is of the order 1, the largest defect scales as  $n_{\text{largest}} = -d(\log L / \log p)$  and the failure stress is proportional to  $n_{\text{largest}}^{-1/\mu}$ . The exponent  $\mu$  may vary between 1 and 4, depending on the dimensionality and the interactions involved. In principle these considerations were already made in Ref. 30. Arguments that lead to this scaling behavior are based on the scaling behavior of a typical defect size that is responsible for global failure. In our case it leads to a height dependence at constant base area, according to

$$\sigma_{\text{fail}} \propto \left( \log \frac{h}{\xi} \right)^{-1/\mu}, \quad (4.1)$$

where  $\xi$  represents the correlation length within the sample. Here the correlation length is a constant within the same base, as can be concluded from the small standard deviation in the coordination number (Table II). In Figs. 5(a) and 5(b) the height dependence of  $\sigma_{\text{fail}}$  is displayed, and it can be

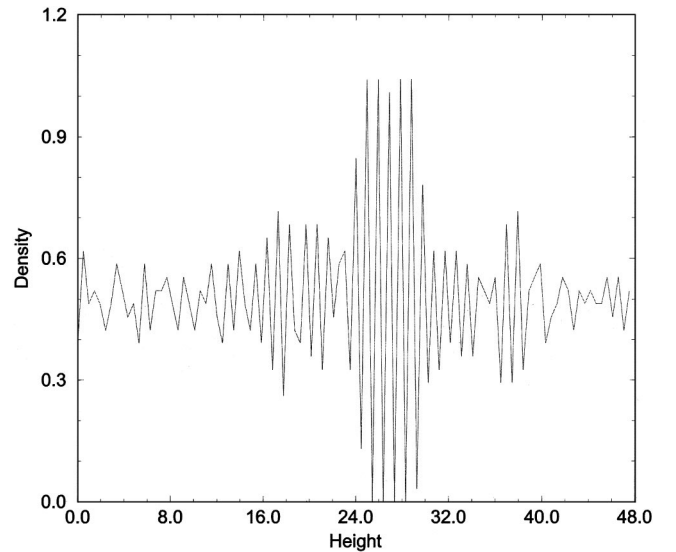


FIG. 4. The density as a function of the sample height (in units of  $0.1 \mu\text{m}$ ) in the case of a composite material.

TABLE III. Heterophase and homogeneous samples (the base area is  $0.64 \mu\text{m}^2$ , and  $C_{\text{Dis}}$  is the homophase system).

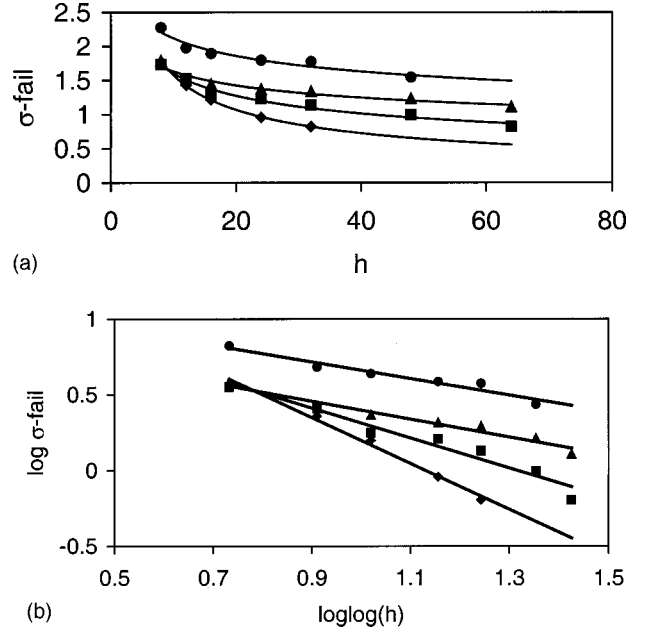
	Homo-phase	Hetero-phase	Homo-phase	Hetero-phase
Height ( $\mu\text{m}$ )	3.2	3.2	4.8	4.8
Height slab ( $\mu\text{m}$ )		0.72		1.9
$C_{\text{Dis}}$		9.0		5.9
$\sigma_{\text{fail}}$ (MPa)	0.82	3.77	0.66	3.72

concluded that  $\sigma_{\text{fail}}$  scales logarithmically with the height, according to Eq. (4.1). It was reported previously<sup>31</sup> that the macroscopic voltage at which a random fuse network fails can be described by a similar logarithmic dependence [Eq. (4.1)], and  $\mu$  was found to be approximately 1.25. However, here  $\mu$  appears to depend sensitively on the system size. In our case  $\mu$  ranges between 0.7 for the smallest system (the base area is  $0.64 \mu\text{m}^2$ ) and 1.8 for the largest system (the base area is  $5.76 \mu\text{m}^2$ ) (see Table II). This sounds reasonable when evaluating the upper and lower bounds of  $\mu$  which depend on the dimensionality  $d$  of the problem and the possible interactions between the local cracks. Within the framework of classical fracture mechanics, with a stress field near the tip of a crack of length  $l$  that scales with the applied stress according to  $\sigma\sqrt{l}$ , the stress fields at a crack tip becomes proportional to  $\sigma n^{1/4}$  (with  $n$  the “size” of the defect) and  $\mu$  is equal to 4 (for a penny-shaped defect of size  $2l$  and  $n = \pi l^2$ ). In general, for systems with noninteracting defects in a network described by central forces,  $\mu = 2(d-1)$ . Indeed, simulation studies of the fracture strength distribution of a two-dimensional 2D triangular network of randomly diluted bond percolating systems showed that a Gumbel distribution with  $\mu = 2$  fits the data better than a Weibull distribution,<sup>32,33</sup> even up to the percolation limit. If in a 2D triangular network bond-bending forces are also included, the same conclusion can be drawn for increasing disorder and  $\mu$  becomes unity.<sup>32</sup> However, for the fracture strength distribution of superelastic 2D networks it was observed that the Weibull distribution gives a better description than the Gumbel distribution.<sup>32</sup>

If the concentration of cracks increases, the interaction between these defects will cause that the stress at the crack tip depends on the size of the defects  $n$ . Assuming a linear scaling, the stress at the crack tip becomes proportional to  $\sigma n$ , and  $\mu$  becomes closer to unity. For smaller systems when local interactions between the defects are more likely to occur, one expects a smaller value for  $\mu$  around unity depending on the details of the force fields in the network. Indeed, an increase of  $\mu$  with sample size to 4 (for central

TABLE IV. Heterophase and homophase samples with an effective height  $h_{\text{eff}}(h - h_{\text{slab}})$ .

$h$ ( $\mu\text{m}$ )	3.2	4.8
$h_{\text{eff}}$ ( $\mu\text{m}$ )	2.5	2.9
$\sigma_{\text{fail}}$ (Mpa) of the disordered phase with $h_{\text{eff}}$	0.94	0.87

FIG. 5. (a) plot of the failure stress (MPa) vs height (in units of  $0.1 \mu\text{m}$ ) for various base areas ( $\diamond$ ,  $0.64 \mu\text{m}^2$ ;  $\blacksquare$ ,  $1.44 \mu\text{m}^2$ ;  $\blacktriangle$ ,  $2.56 \mu\text{m}^2$ ;  $\bullet$ ,  $5.76 \mu\text{m}^2$ ). (b) Plot of the natural logarithm of the failure stress (MPa) vs the double (natural) logarithm of the height [in units of (a)] for various base areas.

forces only) is found in this work (see Table II). It is interesting to note that  $\mu$  for the smallest volumes studied here is 0.7, i.e., much smaller than what one would expect when only central forces are included. This lower value is likely the result of the fact that the total elastic energy is described by two-body central force, three-body bond bending, and four-body torsion contributions. It gives rise to a more substantial overlap of localized stress fields for smaller sizes. Because of the size dependence of  $\mu$ , one should be careful to extrapolate these findings, as cast in Eq. (4.1), to all kinds of microstructures and composite materials. Only for highly porous ceramic materials that show brittle failure, a size dependence of the failure stress described by Eq. (4.1) is experimentally confirmed. Because of plasticity this is not the case for comparable structures like metallic foams, in which failure mechanisms even differ in compression (buckling of the struts) compared to tension (fracture of the struts). Thus the overall size dependence, including the size dependence of  $\mu$ , is strongly affected by the type of failure mechanism and the local microstructure, as reflected in Table II by the coordination number. Further, it may be argued that Eq. (4.1) is actually more complex and that  $\mu$  could still be considered to be independent of the sample size, and thus the logarithmic dependence is only the leading term in this equation. Thus, the values of  $\mu$  listed in Table II are actually effective values, and within the same kind of failure mechanism and microstructure the exponent  $\mu$  becomes more or less universal. However, it would be necessary to include correction terms that cannot really be neglected for other systems. Such correction-to-scaling terms can be quite significant (see, for example, Refs. 8 and 32). Actually, Fig. 5(b) already hints at such a possibility, as the log of the stress failure versus the



double log of  $h$  does not really produce a perfect straight line for the case of a base area of  $1.44 \mu\text{m}^2$ .

In conclusion, we may state that the modulus  $\mu$  in the Gumbel failure distribution appears to depend on the system size because of the decrease of interactions between the defects with increasing height. However, in all cases thin (in the loading direction) samples are stronger than thick samples under uniaxial compression, and the failure stress increases with increasing coordination number. If the height is increased, the onset of ultimate failure takes place earlier because the number of possible critical crack paths is increased. Within the framework of the weakest-link principle, we may say that with increasing size the weakest link will be weaker. Therefore, the strength decreases with increasing height, and this will ultimately lead to a vanishing strength at infinite thickness. With an increasing base area, i.e., for broader samples, the chance that fracture is initiated in a larger sample is also larger than in a smaller sample. However, the load bearing capacity increases with the sample width, and the results in a finite strength for an infinitely broad sample. The latter can also be argued based on classical fiber bundle models.<sup>34</sup>

Further, it can be concluded that the failure stress of a composite material differs considerably from that of a homophase materials (see Table IV). The composite materials show an increase in strength by a factor of 4 in comparison with the disordered structures of the same size. The actual enhancement in strength due to the slab depends on the thickness of the slab. In fact, the size of a heterophase sample could be chosen to be 15–25 times larger than a homophase disordered structure while retaining the same strength. However, the actual failure stress of the composite material depends critically on the details of the configuration. Figure 4 shows a layering effect of the disordered region near the ordered phase, together with the formation of clusters in the disordered phase. In Fig. 6 the layering and clustering effects are also visible for the case of a heterophase three-dimensional network with a base area of  $0.64 \mu\text{m}^2$  and height of  $4.8 \mu\text{m}$ . This layering effect in the radial distribution is similar to the observation of density oscillations at liquid surfaces in bulk recrystallization and surface melting, found both experimentally<sup>35,36</sup> and theoretically.<sup>37,38</sup> The solid induces a layerlike density oscillation in the liquid with a periodicity that depends on the wave vector where the structure factor has its strongest peak. The density profile of Fig. 4 as a function of the distance  $r$  from the interface at  $r_0$  can be described by

$$\rho(r) = \rho_0 + 0.5 \left\{ e^{-(r-r_0)/\lambda} \cos \left[ \frac{2\pi}{a} (r-r_0) \right] \right\}, \quad (4.2)$$

where  $\rho_0$  is the density fluctuation of the disordered phase and  $a$  is the periodicity of the interlayer spacing in the ordered phase.  $\lambda$  is the correlation length in the disordered system, and  $\lambda^{-1}$  reflects the degree of disorder at the inter-

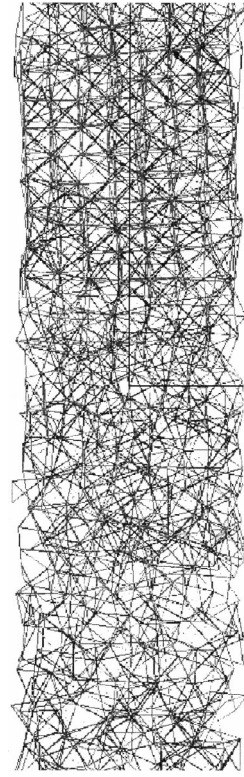


FIG. 6. A heterophase three-dimensional network: the base area is  $0.64 \mu\text{m}^2$ , and the height is  $4.8 \mu\text{m}$ .

face. The form of Eq. (4.2) is typically what one should expect from a mean-field treatment.<sup>39,40</sup> Global fracture of the composite material occurs in the disordered phase because it represents the weakest part of the material. However, because of these layering effects around the interfaces with the ordered phase, i.e., including the ordered clusters that appear in the disordered system, the relevant height for fracture is much smaller than the height simply described by  $h_{\text{eff}} = h - h_{\text{slab}}$ . On average, the largest height of the fully disordered phase in Fig. 4 is about  $0.5 \mu\text{m}$  (also see Fig. 6), corresponding to a failure stress of at least 2.5 MPa as estimated from Fig. 5. This value must be considered as a lower bound because of the details in the configurations. Nevertheless, it is much closer to the actual result of the calculation (Table III) than predictions based on  $h_e - h_{\text{slab}}$  (Table IV), and it underlines the importance of the density fluctuations near the various interfaces in these composite materials.

#### ACKNOWLEDGMENTS

The work described in this paper, part of the research program of the foundation for Fundamental Research on Matter (FOM Utrecht), was supported by the Netherlands Organization for Scientific Research (NWO—The Hague). The authors are grateful to Dr. E. F. Botta and Dr. A. Van der Ploeg for providing us with the matrix solver.



\*Email address: hossonj@phys.rug.nl

- <sup>1</sup>I. C. van den Born, A. Santen, H. D. Hoekstra, and J. Th. M. De Hosson, Phys. Rev. B **43**, 3794 (1991).
- <sup>2</sup>B. K. Chakrabarti and L. Gilles Benguigui, *Statistical Physics of fracture and breakdown in disordered systems* (Clarendon, Oxford, 1997).
- <sup>3</sup>J. W. Chung, A. Roos, J. Th. M. De Hosson, and E. van der Giessen, Phys. Rev. B **54**, 15 094 (1996).
- <sup>4</sup>I. C. van den Born, A. Santen, H. D. Hoekstra, and J. Th. M. De Hosson, in *Fracture Processes in Concrete, Rock and Ceramics*, edited by J. J. M. van Mier, J. G. Rots, and A. Bakker (E & FN SPON, London, 1991), p. 231.
- <sup>5</sup>S. Feng, P. N. Sen, B. I. Halperin, and C. J. Lobb, Phys. Rev. B **30**, 5386 (1984).
- <sup>6</sup>H. J. Hermann, A. Hansen, and S. Roux, Phys. Rev. B **39**, 637 (1989).
- <sup>7</sup>S. Arbabi and M. Sahimi, Phys. Rev. B **38**, 7173 (1988).
- <sup>8</sup>M. Sahimi and S. Arbabi, Phys. Rev. B **47**, 695 (1993).
- <sup>9</sup>S. Arbabi and M. Sahimi, Phys. Rev. B **41**, 772 (1990).
- <sup>10</sup>S. Arbabi and M. Sahimi, Phys. Rev. B **38**, 7173 (1988).
- <sup>11</sup>S. Arbabi and M. Sahimi, Phys. Rev. Lett. **65**, 725 (1990).
- <sup>12</sup>J. Wang, J. Phys. A **22**, L291 (1989).
- <sup>13</sup>S. Arbabi and M. Sahimi, J. Phys. A **23**, 2211 (1990).
- <sup>14</sup>B. Kahng, G. G. Batrouni, S. Redner, L. de Arcangelis, and H. J. Herrmann, Phys. Rev. B **37**, 7625 (1988).
- <sup>15</sup>P. M. Duxbury, P. D. Beale, and C. Moukarzel, Phys. Rev. B **51**, 3476 (1995).
- <sup>16</sup>P. L. Leath and P. M. Duxbury, Phys. Rev. B **49**, 14 905 (1994).
- <sup>17</sup>*Statistical Models for the Fracture of Disordered Media*, edited by H. J. Hermann and S. Roux (North-Holland, Amsterdam, 1990), and references therein.
- <sup>18</sup>M. R. A. van Vliet and J. G. M. van Mier, in *Material Instabilities in Solids*, edited by R. de Borst and E. van der Giessen (Wiley, New York, 1998), p. 185.
- <sup>19</sup>*Size-Scale Effects in the Failure Mechanisms of Materials and Structures*, edited by A. Carpinteri (E&FN SPON, London, 1996), and references therein.
- <sup>20</sup>H. J. C. Berendsen, J. P. M. Postma, W. F. van Gunsteren, A. DiNola, and J. R. Haak, J. Chem. Phys. **81**, 3684 (1984).
- <sup>21</sup>M. P. Allen and D. J. Tildesley, *Computer Simulations of Liquids* (Oxford University Press, Oxford, 1992).
- <sup>22</sup>J. W. Chung, J. Th. M. De Hosson, and E. van der Giessen, Phys. Rev. B **64**, 064202 (2001).
- <sup>23</sup>J.-j. Aue and J. Th. M. De Hosson, J. Mater. Sci. **33**, 5455 (1998).
- <sup>24</sup>W. Weibull, Ingeniörsvetenskapsakademiens, Handlingar, **151**, 1 (1939).
- <sup>25</sup>P. Ray and B. K. Chakrabarti, Solid State Commun. **53**, 477 (1985).
- <sup>26</sup>B. K. Chakrabarti, in *Non-Linearity and Breakdown in Soft Condensed Matter*, edited by K. K. Bardan, B. K. Chakrabarti, and A. Hansen, Lecture Notes in Physics Vol. 437 (Springer, Heidelberg, 1994), p. 171.
- <sup>27</sup>W. I. Newman and A. M. Gabrielov, Int. J. Fract. **50**, 1 (1991).
- <sup>28</sup>E. J. Gumbel, *Statistics of Extremes* (Columbia University Press, New York 1958).
- <sup>29</sup>D. Stauffer, *Introduction to Percolation Theory* (Taylor and Francis, London, 1985).
- <sup>30</sup>P. M. Duxbury, P. L. Leath, and P. D. Beale, Phys. Rev. **36**, 367 (1987).
- <sup>31</sup>B. Kahng, G. G. Batrouni, S. Redner, L. de Arcangelis, and H. J. Hermann, Phys. Rev. B **37**, 7625 (1988).
- <sup>32</sup>M. Sahimi and S. Arbabi, Phys. Rev. **77**, 713 (1993).
- <sup>33</sup>P. D. Beale and D. Srolovitz, Phys. Rev. **37**, 5500 (1988).
- <sup>34</sup>H. E. Daniels, Proc. R. Soc. London, Ser. A **83**, 404 (1945).
- <sup>35</sup>H. Reichert, O. Klein, H. Dosch, M. Denk, V. Honkilmaki, T. Lippmann, and G. Reiter, Nature (London) **408**, 839 (2000).
- <sup>36</sup>W. J. Huisman, J. F. Peters, M. J. Zwanenburg, S. A. de Vries, T. E. Derry, D. Abernathy, and J. F. van der Veen, Nature (London) **390**, 379 (1997).
- <sup>37</sup>R. L. Davidchack and B. B. Laird, J. Chem. Phys. **108**, 9452 (1998).
- <sup>38</sup>J. Q. Broughton and G. H. Gilmer, J. Chem. Phys. **84**, 5749 (1986).
- <sup>39</sup>O. Tomagnini, F. Ercolessi, S. Iarlori, F. D. Di Tolla, and E. Tosatti, Phys. Rev. Lett. **76**, 1118 (1996).
- <sup>40</sup>P. Tarazona and L. Vidente, Mol. Phys. **56**, 557 (1985).